Rapid time-gated polarimetric Stokes imaging using photoelastic modulators

Sanaz Alali,[1,*] Tianyu Yang,[1,2] and I. Alex Vitkin[1,3]

[1]*Division of Biophysics and Bioimaging, Ontario Cancer Institute/University Health Network and Department of Medical Biophysics, University of Toronto, 610 University Avenue, Toronto, Ontario M5G 2M9, Canada*

[2]*Electrical and Computer Engineering, University of Toronto, 10 King's College Road, Toronto, Ontario M5S 3G4, Canada*

[3]*Department of Radiation Oncology, University of Toronto, 610 University Avenue, Toronto, Ontario M5G 2M9, Canada*

**Corresponding author: sanaz.alali@mail.utoronto.ca*

Received May 31, 2013; revised July 9, 2013; accepted July 9, 2013;
posted July 9, 2013 (Doc. ID 190552); published August 7, 2013

We report a rapid time-gated full Stokes imaging approach without mechanically moving parts, which is well-suited for biomedical applications, using two photoelastic modulators (PEMs). A charge-coupled device (CCD) with microsecond time-gating capability was used to acquire the images. To synchronize the CCD with the PEMs, thus gaining signal-to-noise ratio advantage, a field programmable gate array was employed. After calibration, an evolutionary algorithm was used to select four time points from which the full Stokes vector can be recovered. Using the images taken by the camera at these four times (in ~80 ms), the images of the full Stokes vectors of different incident polarization states were accurately derived.

OCIS codes: (110.5405) Polarimetric imaging; (170.6935) Tissue characterization.
http://dx.doi.org/10.1364/OL.38.002997

Polarized light is frequently used in biomedical applications for assessing tissue morphology [1,2]. For examining tissues that are spatially heterogeneous, large fields of view and high resolution are desirable, necessitating an imaging approach. Moreover, image acquisition time should be minimized to avoid *ex vivo* tissue alterations and *in vivo* motion artifacts. Recently, snapshot polarimetric imaging systems have been reported using gratings and prisms [3,4]. Although fast, these methods apply spatial frequency filters, reducing the information content of the image. Other potential rapid polarimetric imaging systems, based on photoelastic modulators (PEMs) or liquid-crystal (LC) modulators, offer higher resolution with large fields of view, and are thus potentially more suitable for biomedical imaging [5–10]. Mueller matrix imaging with LCs is achievable in a few seconds [5,6]. But PEMs are faster, have larger apertures, and have larger retardance modulation amplitudes than the LCs [10]. In addition, high signal-to-noise ratio (SNR) is achievable when the data acquisition is synchronized with the PEM frequency, for example, via lock-in amplifiers coupled to a point-sensing detector such as a photodiode or a photomultiplier [7–11]. However, a rapid high SNR no-moving-parts full Stokes imaging system based on a charge-coupled device (CCD), and without a prior simplifying assumption about the polarization states, has not been developed yet.

Using one PEM and applying the stroboscopic technique, Han and Chao imaged the Mueller matrix of thin films that have several zero elements and a known mathematical form [7]. However, this technique cannot be applied to turbid media with an unknown Mueller matrix. Also, for aerosol detection, Diner *et al.* demonstrated a dual PEM imager that only measures the linear portions of the Stokes vector [8], again insufficient for proper turbid media characterization. Here, we demonstrate rapid full Stokes vector imaging with two PEMs using optical gating with a CCD camera in the time domain. We optimize the CCD measurement times relative to the phase modulations induced by the two PEMs; then, to overcome the experimental reality of PEMs' slight frequency drifts, we demonstrate the use of a field programmable gate array (FPGA) to trigger the CCD whenever the two PEMs are at a specified relative phase in their modulation cycles. Unlike previous methods, we make no simplifying assumptions on the polarization states and are able to recover the full Stokes vector images from only four temporally selected CCD frames, all within milliseconds.

We use a CCD and an FPGA to acquire full Stokes images from a dual PEM system as shown in Fig. 1. The two PEMs (Hinds Instruments), PEM_1 with $f_1 = 20.07$ kHz at 0° modulation axis orientation and PEM_2 with $f_2 = 42.06$ kHz at 45°, and a horizontally oriented linear polarizer P_2, constitute the polarization state analyzer (PSA) [8–10,12–14]; the methodology is of course not restricted to these specific parameter values. Each PEM induces a retardance $\delta_i(t)$ according to

$$\delta_i(t) = \delta_o \sin(2\pi \times f_i t + \varphi_i), \tag{1}$$

where δ_o was set to 3.142 for both PEMs, f_i is the modulation frequency, and ϕ_i is a phase. The light source was a

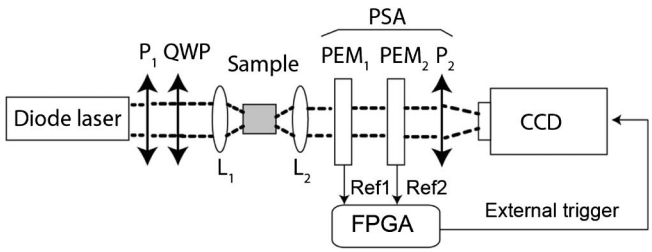

Fig. 1. Time-gated PEM Stokes imaging with two PEMs. The linear polarizer P_1 and the removable quarter-wave plate (QWP) change the incident light polarization on the sample. PEM_1 and PEM_2 and linear polarizer P_2 constitute the PSA. The FPGA provides the external trigger for the CCD from the reference frequencies of the two PEMs. L_1 and L_2 are lenses.

cw diode laser (Coherent) at a wavelength of 641 nm and a maximum power of 100 mW, and a spot size of about 2 mm was used. The polarization state entering the PSA was determined by another linear polarizer, a removable quarter-wave plate (QWP), and the sample polarization properties (if any). The CCD camera (PI-max III Princeton Instruments) registered 152 × 152 pixel images with a resolution of 50 μm per pixel. Defining the Stokes vector of light after interaction with the sample upon entering the PSA as S_{in}, the time-dependent Stokes vectors at the camera, S_{out}, can be written as

$$S_{\text{out}}(t) = \begin{pmatrix} I(t) \\ Q(t) \\ U(t) \\ V(t) \end{pmatrix} = M_{P2} M_{\text{PEM2}}(t) M_{\text{PEM1}}(t) S_{\text{in}}, \quad (2)$$

where $I(t)$ is the intensity, and $Q(t)$, $U(t)$, and $V(t)$ are the linear polarization at 0° or 90°, the linear polarization at 45° or −45°, and the circular polarizations, respectively. M_{PEMi} and M_{P2} are the Mueller matrices of the ith PEM and the polarizer P_2. The PEMs and the polarizer in the PSA enable the CCD to image light with the polarization with a Stokes vector $S_A(t) = [a_1(t) \quad a_2(t) \quad a_3(t) \quad a_4(t)]^T$, which is the transpose of the first row of the $M_{P2} M_{\text{PEM2}} M_{\text{PEM1}}$ matrix. Hence, $I(t)$ at any time t_k registered by the CCD can be rewritten as

$$I(t_k) = [a_1(t_k) a_2(t_k) a_3(t_k) a_4(t_k)] S_{\text{in}}. \quad (3)$$

At different time points t_1, t_2, t_3, and t_4, we can rewrite the four time-dependent CCD-detected signal intensities in matrix form as

$$\begin{pmatrix} I(t_1) \\ \vdots \\ I(t_4) \end{pmatrix} = A S_{\text{In}} = \begin{bmatrix} a_1(t_1) & a_2(t_1) & a_3(t_1) & a_4(t_1) \\ a_1(t_2) & a_2(t_2) & a_3(t_2) & a_4(t_2) \\ a_1(t_3) & a_2(t_3) & a_3(t_3) & a_3(t_3) \\ a_1(t_4) & a_2(t_4) & a_3(t_4) & a_4(t_4) \end{bmatrix} S_{\text{In}}. \quad (4)$$

By choosing $t_1, \ldots, t_4$ to ensure a nonsingular system matrix A, the Stokes vector S_{in} is retrieved from the direct product of the inverse of matrix A and the acquired intensities as

$$S_{\text{in}} \equiv A^{-1} \begin{pmatrix} I(t_1) \\ \vdots \\ I(t_4) \end{pmatrix}. \quad (5)$$

For such a system, the lower the condition number of A, the more accurate the recovered solution [13–17]. For an LC-based polarimetric system, Aas *et al.* used a genetic algorithm to optimize the LCs' parameters [15]. We use a similar approach here to find the times $t_1, \ldots, t_4 (0 < t_i <$ common period of oscillation $= 500$ μs) that yield a nonsingular matrix A with minimum condition number $\kappa(A) = \|A\| \cdot \|(A)^{-1}\|$, with $\|\|$ being the second degree norm [16]. We use an adapted version of the evolutionary algorithm (EA) proposed in [18]. This EA starts from a random (parent) solution vector $t_1, \ldots, t_4$ and generates a population of offsprings using cross-mutation and self-mutation techniques [18]. In each step, the condition number of the matrix A is calculated for all the vectors in the population. If any vector is fitter (its $\kappa(A)$ is smaller) than the parent vector, it survives and becomes the parent solution vector.

However, selecting the times $t_1, \ldots, t_4$ is challenging because of the frequency drift of the real-life PEMs [8,10]. Due to this drift, the phases $\phi_i s$ in Eq. (1) randomly change with time and change the system matrix A through Eqs. (1)–(5); indeed, selecting $t_1, \ldots, t_4$ to minimize $\kappa(A)$ is meaningful only when the phases of the PEMs' modulation relative to each other are known. We address this challenge by employing an FPGA in what we are calling a sequential time-gating approach. An Altera DE2 FPGA was used to generate a trigger pulse for the CCD when the two PEMs were in certain fixed relative phase ϕ_o. Each PEM controller generates a 5 Vpp square wave at its modulation frequency. The square wave output of the PEMs' controllers and camera's external trigger were connected to a FPGA as shown in Fig. 1. A 32-bit 50 MHz FPGA counter was used to track the time of the rising and falling edges of each square wave. As shown in Fig. 2(a), a trigger pulse was sent to the camera if the rising edge of one of the square waves and the falling edge of the other one took place within three FPGA clock cycles (time difference of $\Delta t < 60$ ns), which determines the value of ϕ_o when the trigger is sent [Fig. 2(a)]. The CCD should then acquire an image when it receives the trigger; however, there is another experimental variable, a short unwanted electronic delay t_o before it starts acquiring an image as depicted in Fig. 2(b).

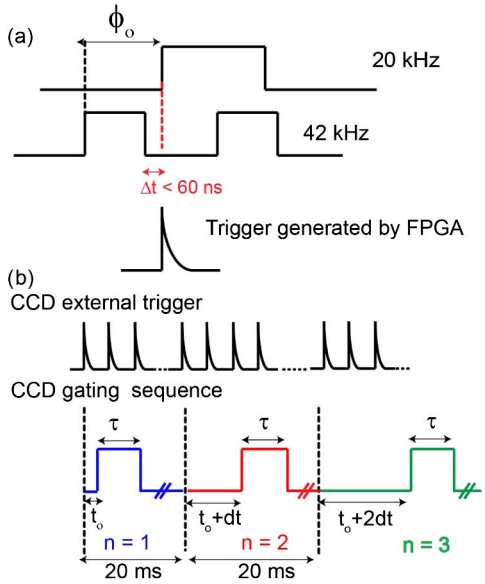

Fig. 2. (a) Trigger pulse is generated by FPGA when rising edge and falling edge of the PEMs are within 60 ns. At the rising edge of the trigger, the PEMs have a phase difference of ϕ_o. (b) CCD gates the incoming intensity for $\tau = 0.5$ μs in each exposure n. Gating times for consequent images are programmed to be delayed with multiples of $dt = 0.5$ μs with respect to the trigger. t_o is a short unwanted electronic delay of the CCD with respect to the trigger. Acquiring each image takes 20 ms.

To capture the intensity variation in microsecond time, the CCD was programmed to gate (~embedded electronic shutter) the intensity for a time $\tau = 0.5$ μs, after a user-defined delay of $(n-1)\times dt = (n-1)\times 0.5$ μs from the trigger pulse, in each exposure n, as illustrated in Fig. 2(b). As seen, while the trigger is generated rapidly, the CCD acquires each image after receiving the trigger and only if it is finished registering the previous frame. As an example, registering each 152×152 pixel frame takes about 20 ms. With this acquisition scheme, the time-varying retardances of the PEMs are

$$\delta_1(t) = 3.142\,\sin(2\pi\times 20.07\times 10^3(t+t_o)+\varphi_o),$$
$$\delta_2(t) = 3.142\,\sin(2\pi\times 42.06\times 10^3(t+t_o)). \quad (6)$$

To exactly measure t_o and ϕ_o in Eq. (6), the intensities of four known incident Stokes vectors were measured: the linear polarizations 0°, 45°, and 90° and the right circular polarization, all generated by rotating the polarizer P_1 manually plus adding a QWP for the right circular polarization through air (i.e., Fig. 1 with the sample removed). A sequence of $n = 1000$ images [$t = 0$–500 μs in Eq. (6)] was acquired by the CCD. The registered intensities for the incident linear 45° and right circular polarizations are shown in Figs. 3(a) (Media 1) and 3(b) (Media 2). The mean value of 10 central pixels of the image sequence was calculated for these two cases, as plotted in black over 250 μs in Figs. 3(c) and 3(d). By scanning different values of t_o and ϕ_o, the maximum cross-correlation coefficient between the theoretical [from Eqs. (2)–(6)] and the measured intensities was obtained when $t_o = 87$ μs and $\phi_o = -1.2915$ rad. The correlation coefficients between measured and simulated intensities were 0.99 for 0° and 90° polarizations, 0.98 for 45° polarization, and 0.93 for right circularly polarized light. Corresponding theoretical predictions for $I(t)$ are plotted in red in Figs. 3(c) and 3(d), showing excellent agreement between experiments and simulations. The experimental results shown in Fig. 3 are robust, exhibiting ~1% variation over repeated acquisitions during different days. This verifies that the values of t_o and ϕ_o are ~constant regardless of the PEMs' frequency drifts, and suggests SNR boosts via repeated acquisitions and averaging.

Next, the exact retardance of the PEMs from Eq. (6) was fed to the EA to obtain the optimum $t_1,\ldots,t_4$, which gave the minimum condition number $\kappa(A)$. The resulting values of $t_1,\ldots,t_4$ and $\kappa(A)$ are shown in Table 1; $\kappa(A)$ magnitude is comparable to condition numbers reported in [12,14], suggesting a stable solution. The system matrix A was then used via Eq. (5) to recover the incident Stokes vectors images for different incidences, using the images acquired at t_1, t_2, t_3, and t_4 of Table 1.

Figure 4 presents the correctly recovered Stokes images when the incident beam polarization varies. Mean value of degree of polarization, $((Q^2+U^2+V^2)^{1/2}/I)$ of these Stokes vectors is 97%. Note that whereas we used the entire period (1000 frames) for the calibration purposes, here we only used four images that took a mere 4×20 ms $= 80$ ms.

To test system performance in a biomedical setting, we imaged 0.6 mm thick of frozen chicken breast

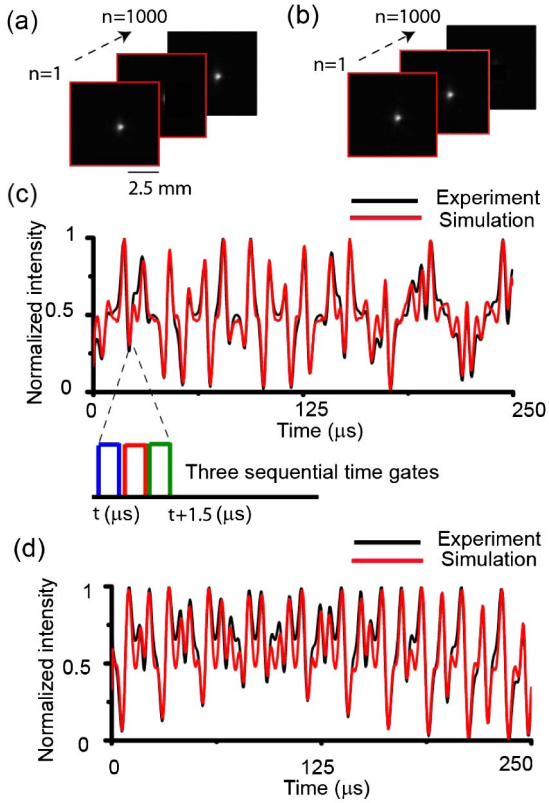

Fig. 3. Experimental image sequence over 500 μs (one period) acquired by the CCD, using FPGA assisted sequential time gating, when the incident light is (a) linearly polarized at 45° (Media 1), (b) right circularly polarized (Media 2). (c) Mean value of 10 central pixels in (a) over 250 μs shown in black, and the simulation from Eqs. (2)–(6) when S_{in} is linearly polarized at 45° plotted in red. We also illustrate how the entire signal is sampled sequentially (only three consequent gating times shown, each 0.5 μs), as suggested by Fig. 2. (d) Analogous figure for right circularly polarized incidence from the 10 central pixels of the time-varying image of (b).

that is birefringent and has a transport albedo (= reduced scattering coefficient/(reduced scattering coefficient + absorption coefficient) of 0.9 [19]. The degree of polarization of the incident Stokes vector (0° polarization) and that after interaction with the chicken breast were calculated and shown in Figs. 5(b) and 5(c). As expected, there is a significant depolarization after interaction with the scattering sample, and its magnitude fits well into the depolarization/optical properties trend established and validated in our previous study [20].

In conclusion, we demonstrated a fast dual-PEM imaging scheme for full Stokes polarimetry of turbid media. To account for experimental complications of PEM frequency drifts, we used an FPGA to trigger the CCD when the two PEMs are in certain phase relative to each other. Then, applying the EA, we determined the four

Table 1. Optimum $t_1,\ldots,t_4$ in Microseconds Derived from EA, and the Corresponding Condition Number $\kappa(A)$

t_1	t_2	t_3	t_4	$\kappa(A)$
58.5	92	118	291	1.78

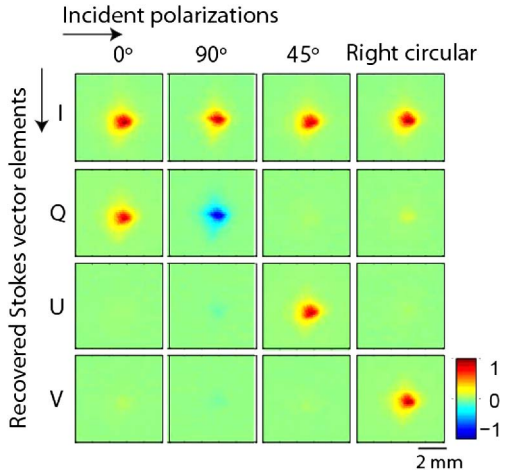

Fig. 4. Experimentally recovered images of the Stokes elements from four different incident polarizations (no sample in Fig. 1). The rows I, Q, U, and V indicate the resulting Stokes vector element images (120 × 120 pixels).

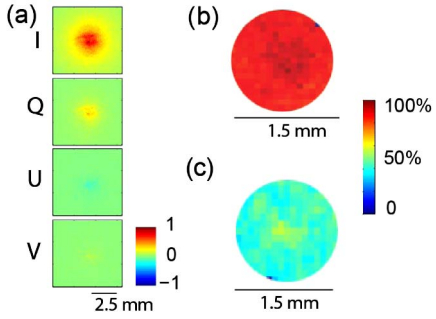

Fig. 5. (a) Stokes images of light transmitted through a 1.2 mm thick frozen chicken breast with 0° linear polarization illumination. Polarization degree of (b) incident linearly polarized beam and (c) Stokes vector after interacting with the chicken breast slab in (a).

time points at which the matrix that describes the system has a low condition number. The CCD registered microsecond resolved time-gated images at those four times in synchronization with the PEMs. By multiplying these four time-gated images by the inverse of the system's matrix, we recovered the full Stokes vector images, verified the system performance and accuracy for known input states, and demonstrated its operation in a typical biomedical imaging scenario. Importantly, this scheme can be expanded to a four-PEM Mueller matrix imaging scheme that can recover the full polarimetric images of the 16 elements in a millisecond time frame. Theoretical details of this approach are presented in a separate article [21].

References

1. V. V. Tuchin, *Tissue Optics*, 2nd ed. (SPIE, 2007).
2. S. L. Jacques, J. R. Roman, and K. Lee, Lasers Surg. Med. **26**, 119 (2000).
3. H. Luo, K. Oka, E. DeHoog, M. Kudenov, J. Schiewgerling, and E. L. Dereniak, Appl. Opt. **47**, 4413 (2008).
4. M. W. Kudenov, M. J. Escuti, N. Hagen, E. L. Dereniak, and K. Oka, Opt. Lett. **37**, 1367 (2012).
5. L. M. S. Aas, P. G. Ellingsen, M. Kildemo, and M. Lindgren, J. Mod. Opt. **57**, 1603 (2010).
6. A. Pierangelo, S. Manhas, A. Benali, C. Fallet, J. L. Totobenazara, M. R. Antonelli, T. Novikova, B. Gayet, A. De Martino, and P. Validire, J. Biomed. Opt. **18**, 046014 (2013).
7. C. Y. Han and Y. F. Chao, Rev. Sci. Instrum. **77**, 023107 (2006).
8. D. J. Diner, A. Davis, B. Hancock, S. Geier, B. Rheingans, V. Jovanovic, M. Bull, D. M. Rider, R. A. Chipman, A. B. Mahler, and S. C. McClain, Appl. Opt. **49**, 2929 (2010).
9. R. C. Thompson, J. R. Bottiger, and E. S. Fry, Appl. Opt. **19**, 1323 (1980).
10. O. Arteaga, J. Freudenthal, B. Wang, and B. Kahr, Appl. Opt. **51**, 6805 (2012).
11. M. F. G. Wood, X. Guo, and I. A. Vitkin, J. Biomed. Opt. **12**, 014029 (2007).
12. G. E. Jellison and F. A. Modine, Appl. Opt. **36**, 8190 (1997).
13. K. M. Twietmeyer and R. A. Chipman, Opt. Express **16**, 11589 (2008).
14. E. Compain, S. Poirier, and B. Drévillon, Appl. Opt. **38**, 3490 (1999).
15. L. M. S. Aas, P. G. Ellingsen, B. E. Fladmark, P. A. Letnes, and M. Kildemo, Opt. Express **21**, 8753 (2013).
16. A. Ambirajan and D. C. Look, Opt. Eng. **34**, 1656 (1995).
17. J. S. Tyo, Opt. Lett. **25**, 1198 (2000).
18. F. Massoumian, S. Alali, and T. Mansouri, Opt. Lett. **34**, 67 (2009).
19. W. F. Cheong, S. A. Prahl, and A. J. Welch, IEEE J. Quantum Electron. **26**, 2166 (1990).
20. S. Alali, M. Ahmad, M. A. Kim, N. Vurgun, M. F. Wood, and I. A. Vitkin, J. Biomed. Opt. **17**, 045004 (2012).
21. S. Alali and I. A. Vitkin, "Optimization of rapid Mueller matrix imaging of turbid media using four photoelastic modulators without mechanically moving parts," Opt. Eng., submitted for publication.